Tribology Letters (2019) 67:87
https://doi.org/10.1007/s11249-019-1196-1

ORIGINAL PAPER

Influence of Frictional Interface State on Tribological Performance of Sintered Polycrystalline Diamond Sliding Against Different Mating Materials

Wenbo Qin[1] · Yaoyao Liu[1] · Wen Yue[1,2] · Chengbiao Wang[2,3] · Guozheng Ma[4] · Haidou Wang[4]

Received: 10 April 2019 / Accepted: 19 June 2019

Abstract
Understanding the evolution of frictional interface state is of great significance to the effective design of antifriction and wear resistance properties at macro-scale contact, which plays an important role in the whole tribological performance. The trigological behavior of the sintered polycrystalline diamond (PCD) sliding against different mating materials was evaluated under dry nitrogen (N_2) environment. The coefficients of friction (COF) and wear rates of the PCD were diverse due to the various formations of transferflim and filling effects across sliding interfaces, which is dependent on the mating materials. Additionally, the Raman measurements demonstrate that the carbon rehybridization (sp^3 to sp^2) process occurred accompanying with the formation of carbonaceous transferfilm during sliding. The effects of antifriction transferfilm formations and filling on the enhanced tribological performance of PCD at macro-scale contact were highlighted.

Keywords Polycrystalline diamond · Transferfilm formation · Carbon rehybridization · Filling effects · Enhanced tribological performance

1 Introduction

The sintered polycrystalline diamond combines a variety of attractive properties such as wear resistance, high hardness and excellent toughness, which makes it suitable for applications in cutting, drilling bits and bearings [1–4]. To achieve further applications, a detailed understanding of the tribological properties and structural evolution of PCD is required [5, 6]. Considerable research efforts have been devoted to the tribological properties of PCD under various complex conditions [7–12]. In our previous work, it indicated that an ultralow friction coefficient regime coincided with the formation of carbonaceous transferfilms was achieved [2]. Following this, it successfully controlled the wear behavior of PCD via altering humidity [13]. During sliding, the overall tribological properties of PCD can be controlled by the complex structure and phase evolution at the contact interfaces.

Recently, for sliding interfaces, many studies have researched the antifriction transferfilm formation including the introduction of two-dimensional material, which can drastically reduce the wear loss and improve antifriction performance [14–18]. It is worthwhile mentioning that the amorphous carbon film transferred to the mating surface contributes a lot to a better anti-wear and friction-reduction behavior [15, 19–21]. This antifriction performance has been still demonstrated in a number of other studies. Waesche et al. [22] explained the difference in tribological performance between soft and hard materials sliding with diamond-like carbon films. A stable transfer layer formed on the alumina counterface plays a key role in reducing friction and wear. In addition, it has been observed that the formation

✉ Wen Yue
yw@cugb.edu.cn; cugbyw@163.com

✉ Chengbiao Wang
cbwang@cugb.edu.cn

1 School of Engineering and Technology, China University of Geosciences (Beijing), Beijing 100083, People's Republic of China

2 Zhengzhou Institute, China University of Geosciences (Beijing), Zhengzhou 451283, People's Republic of China

3 Zhengzhou Institute of Multipurpose Utilization of Mineral Resources, Chinese Academy of Geological Sciences, Zhengzhou 450006, People's Republic of China

4 National Key Lab for Remanufacturing, Academy of Armored Forces Engineering, Beijing 100072, People's Republic of China

Published online: 02 July 2019

of transferfilm successfully alleviated the adhesion effect of PCD in vacuum conditions [9]. Furthermore, the interfacial filling effect can decrease the roughness and then the shear effect can be diminished, which can play an effective role in reducing friction and wear during sliding. Most of previous work has proved that frictional interface state can significantly influence the tribological behavior. Given the importance of interface state in affecting lubrication in sliding process, understanding the relationships among transferfilm formation, filling effects, mating materials and tribological properties are of great significance [23]. Consequently, it is important to highlight the effect of various mating materials on the tribological behavior of PCD, which has a significant effect on choosing suitable tribopairs.

In this work, we studied the friction and wear behavior of PCD sliding against four types of materials in dry N_2 conditions, focusing on their trigological mechanisms and the different sliding interface states. The occurrence of different wear mechanisms has been revealed. Additionally, the evolution of antifriction transferfilm formation, carbon rehybridization process and filling effects were clarified in details, which can induce the enhanced tribological performance of PCD at macro-scale contact.

2 Experimental Procedure

2.1 Fundamental Characteristics of Specimens

The original PCD specimens sintered at Zhongnan Diamond Co., Ltd are composed of a cemented carbide substrate (WC-16 wt% Co) and a polycrystalline diamond layer. Figure 1 shows the structural diagrams of PCD specimens. The thickness of PCD layer is about 0.5 mm. It is obviously found that the original PCD surface contains diamond phase and Co binder. The diamond phase mainly contains big size diamond grains ~ 25 μm, medium size diamond grains ~ 5–15 μm and tiny diamond grains < 5 μm. There are two bonding ways of diamond–diamond bonds (D–D bonds) and diamond–metal–diamond bonds (D–M–D bonds) among diamond grains and Co binders. Four types of domestic commercial mating balls with a diameter 4 mm were selected. Figure 2 exhibits the comparison of hardness values between PCD and mating balls [24, 25].

2.2 Tribological Tests Procedure

Tribological studies were performed under dry N_2 atmosphere at room temperature using a MS-T3000 tribometer with the ball-on-disk contact geometry (Detailed parameters are shown in Fig. 1). The tribological test parameters are displayed in Fig. 1. In order to ensure data stability, the calibration of tangential force was performed regularly. During tribotests, the lateral force was measured with a strain gauge sensor. For tribotests performed in N_2 environment, the testing chamber was initially introduced nitrogen flows and then the relative humidity (RH) decreased to less than 5%. Both the PCD and balls were initially cleaned by sonication in acetone for 30 min, and then ultrasonically cleaned in ethanol for 30 min. To guarantee the stability of data, each tribotest was performed three times. To estimate the wear performance, the wear rates of balls and PCD were calculated as follows:

$$W_R = V/F_n \times L \tag{1}$$

$$V_1 = \frac{\pi h}{6}\left(3r^2 + h^2\right) \tag{2}$$

$$V_2 = 2\pi r \times A \tag{3}$$

$$h = R - \left(R^2 - r^2\right)^{1/2} \tag{4}$$

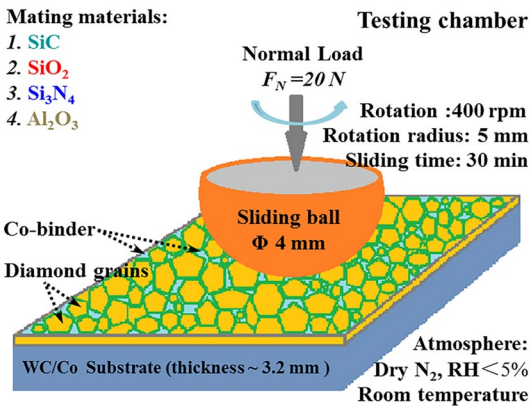

Fig. 1 The structural diagrams PCD layer and the schematic of tribotests

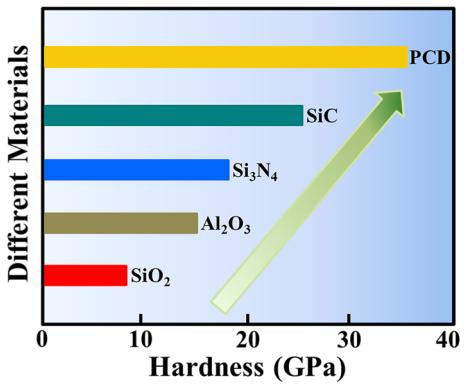

Fig. 2 The comparison of hardness values between PCD and sliding balls

where W_R is the wear rate and it shows the wear volume per unit load and per unit distance, F_n (N) is the applied load, L (mm) is the sliding distance. The wear volumes of the ball and PCD are calculated with the formula V_1, V_2 (mm^3), respectively. R (mm) is the radius of sliding ball, r (mm) is the radius of the wear scar, and h (mm) is the height of the spherical crown. Additionally, A is the cross-sectional area of wear tracks measured by the white light interferometer (NanoMap-D).

2.3 Microanalysis Methods

The optical images of wear scars and tracks were obtained using an optical microscope (Olympus BX51M) with a Nikon camera. The morphologies and wear rates of wear tracks were determined using a NanoMap-D three-dimensional White Light Interferometer. Raman measurement using Lab RAM HR Evolution spectroscopy (HORIBA Jobin–Yvon) was conducted to analyze the evolution of carbon atoms across the sliding interfaces. The Ar + laser wavelength is 532 nm and the laser spot diameter is 1.25 μm. In order to analyze the micro-topographies and element distribution of worn surface, the GeminiSEM-500 field emission scanning electron microscope (SEM) equipped with an energy-dispersive X-ray spectroscope (EDS) was used.

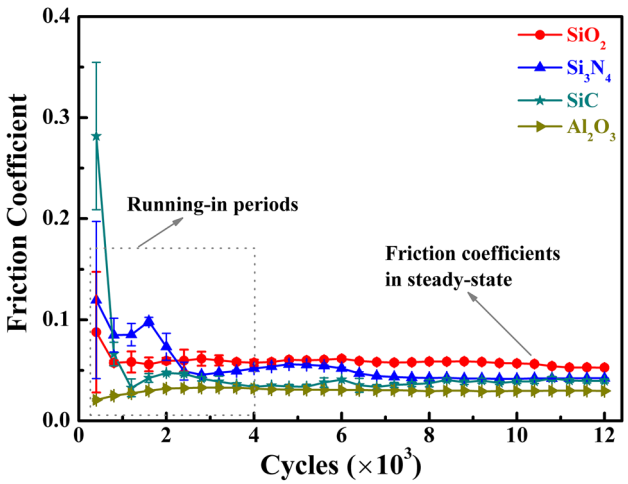

Fig. 3 Coefficients of friction for PCD sliding against different mating materials under N_2 atmosphere at room temperature

3 Results

3.1 Tribological Performances

Figure 3 shows the comparison of the coefficients of friction (COFs) during the whole 12,000 cycles. It is clear that the frictional behavior is strongly influenced by sliding materials. For SiO_2, SiC and Si_3N_4, during initial sliding cycles, the COFs are relatively high and slightly fluctuate, which is corresponding to the running-in period [26]. And then they gradually decreased to a steady-state value. For SiO_2 as the sliding ball, there is a relatively higher COF of ~ 0.06. However, the other balls as mating materials, the COFs are all lower than ~ 0.05 and present a relative steady trend after ~ 6000 cycles. Sliding with Al_2O_3, the COF is the minimum value ~ 0.03, while sliding with SiC and Si_3N_4, the friction coefficients are about ~ 0.04.

Figure 4 displays the optical micrographs of wear scars on the ball surfaces and the corresponding wear tracks formed on the PCD surfaces after tribotests, respectively. There are clearly noticeable worn marks on the sliding ball surfaces. It was found that the wear scar of Si_3N_4 was covered by the colorful transferfilm, while there are gray wear scars formed on SiC and SiO_2 surfaces. Besides, the wear scar of Al_2O_3 is relatively small and clean. Additionally, except for the wear scars of Al_2O_3, a large amount of wear debris is still heaped on the edge regions of wear scars. The corresponding wear tracks of PCD were shown in Fig. 4a1–d1. For the

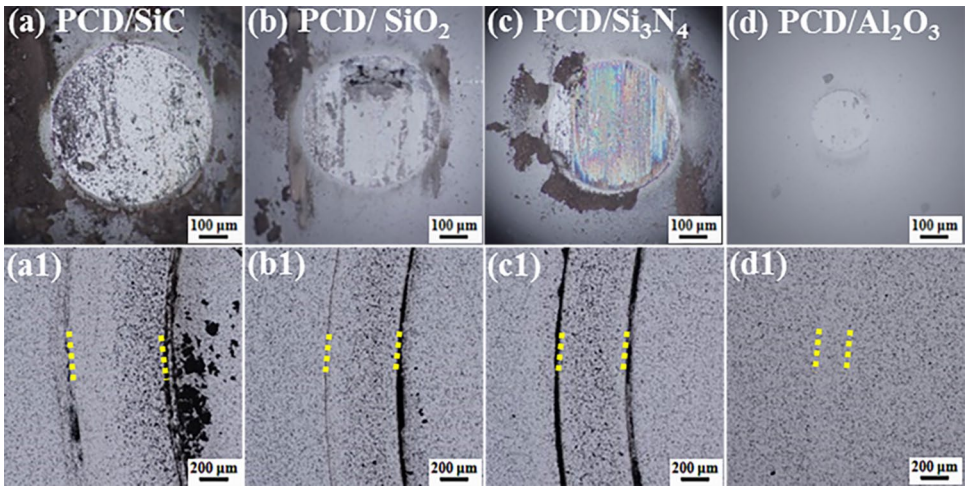

Fig. 4 The optical micrographs of the topography of wear scars: **a–d** and the corresponding wear tracks: **a1–d1**

wear tracks sliding against SiC, SiO_2 and Si_3N_4, there are obvious worn surfaces and wear debris accumulated on both sides of wear tracks.

To further identify the wear performance of PCD, the three-dimensional morphologies of wear tracks are described in Fig. 5. In sliding with SiC, SiO_2, and Si_3N_4, the obvious abrasive worn surfaces can be found. While the Al_2O_3 as mating balls, the wear track on the PCD surface is so superficial that it is hard to be seen. Furthermore, two-dimensional cross-sections of wear tracks are detected to further evaluate the wear rate of PCD, respectively (Fig. 5e). The wear depths of the PCD sliding with SiC, SiO_2 and Si_3N_4 are relatively higher. While sliding with Al_2O_3, the wear depth is so shallow to distinguish. The wear rates of PCD surfaces and sliding balls are summarized in Fig. 6. For sliding with SiC, SiO_2 and Si_3N_4, there are relative higher wear rates for PCD and balls. During dry sliding, the carbon dangling bonds cannot be effectively passivated and the formation of Si–C covalent bonds cannot be avoided, accompanying with the increase of interfacial covalent reactions, which may influence the material removal performance.

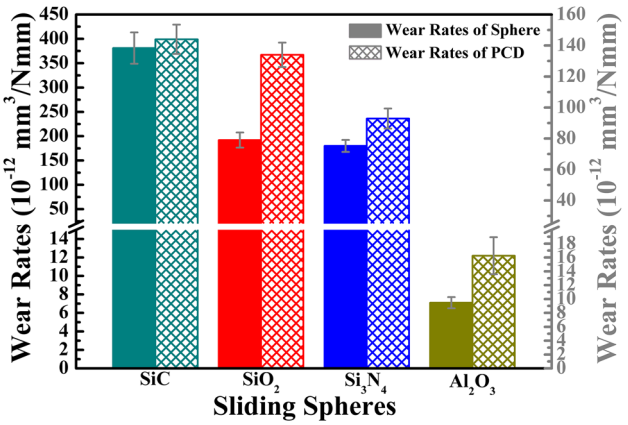

Fig. 6 The comparison of wear rates for PCD and sliding balls. Error bars are standard errors and represent variation within a set of measurements

3.2 Analysis of Carbon Rehybridization

Raman spectra analysis was conducted on wear scars of different mating materials and wear tracks to get a deeper understanding of evolution of carbon atoms during the sliding. As shown in Fig. 7a, apparent signals at ~ 1347.9 cm^{-1} and G-peak at ~ 1578.3 cm^{-1} are detected on the wear scar of Si_3N_4, which is corresponding to graphitic or amorphous carbon structures. The formation of disorder structures play a significantly role in friction reduction [19, 21]. Moreover, this carbon related signal is less obviously detected on wear scars of SiC. Thus, judging from the morphology of the wear scars in Fig. 4, the carbonaceous transferfilm is easily formed on Si_3N_4, but not on SiO_2 and Al_2O_3. Figure 7b depicts a strong peak at 1333.9 cm^{-1} on all wear tracks of PCD, which represents the diamond signal. Meanwhile, peaks at 1550.3 cm^{-1} are also detected at the wear track of PCD after sliding with Si_3N_4 and SiC. The results indicate that the phenomenon of the evolution of material structures occurred during sliding.

3.3 Surface Morphologies of Wear Tracks and Wear Scars

For a better understanding and interpretation of the relationship between the tribological mechanism and mating

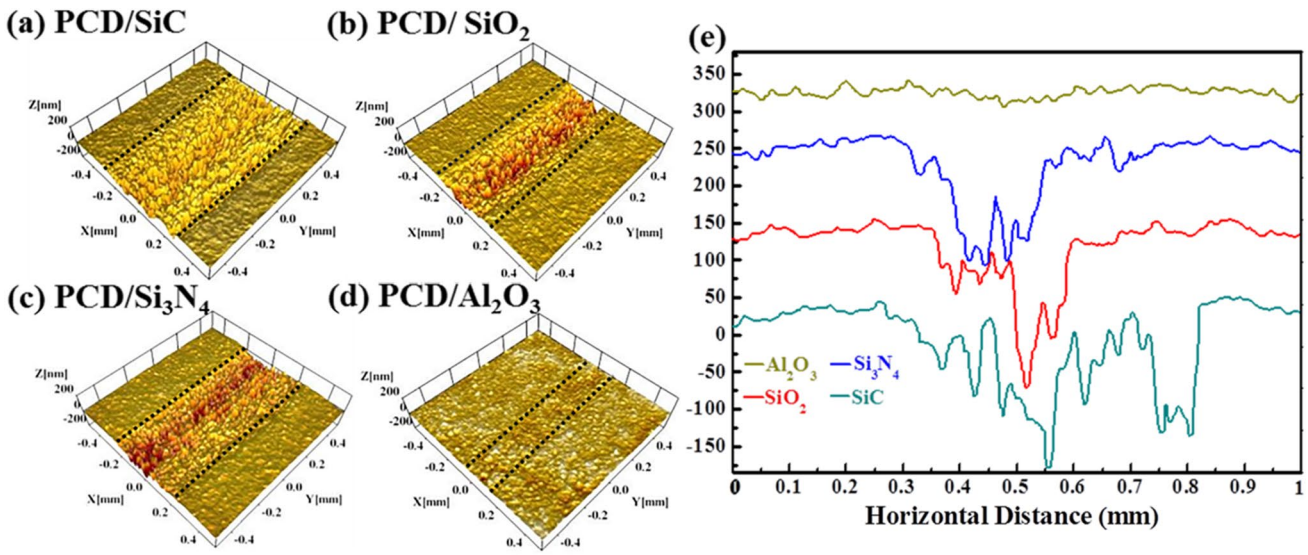

Fig. 5 Three-dimensional optical surface morphologies of wear tracks: **a**–**d** the contrast on its two-dimensional cross-sections (**e**)

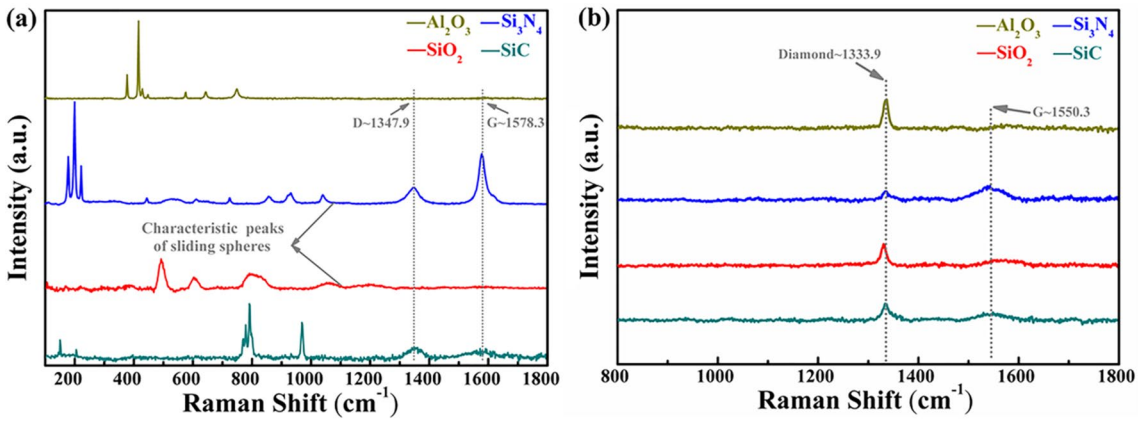

Fig. 7 Raman intensities of worn surfaces: **a** wear scars, **b** wear tracks. It indicates the carbon rehybridization process occurred during sliding accompanying with the formation of carbonaceous transferfilm

materials, scanning electron microscopy and elemental analysis (SEM&EDS) was performed on the worn surfaces of wear tracks and wear scars. The results are shown in Figs. 8 and 9 respectively. Figure 8a shows that PCD surface sliding with SiC presents the most severe wear with the remove of diamond grains. Apparent exfoliated pits as circled by yellow dotted line can be seen from the SEM results. Meanwhile, EDS mapping results demonstrate the padding effect of Si elements at the exfoliated pits, indicating a transfer of materials from sliding balls. In sliding with SiO_2 and Si_3N_4 (Fig. 8b, c), PCD surface shows a less severe exfoliations and transfer phenomenon compared with SiC. Moreover, sliding with Al_2O_3, PCD exhibits a relatively flat surface, under the filling effects of mating materials

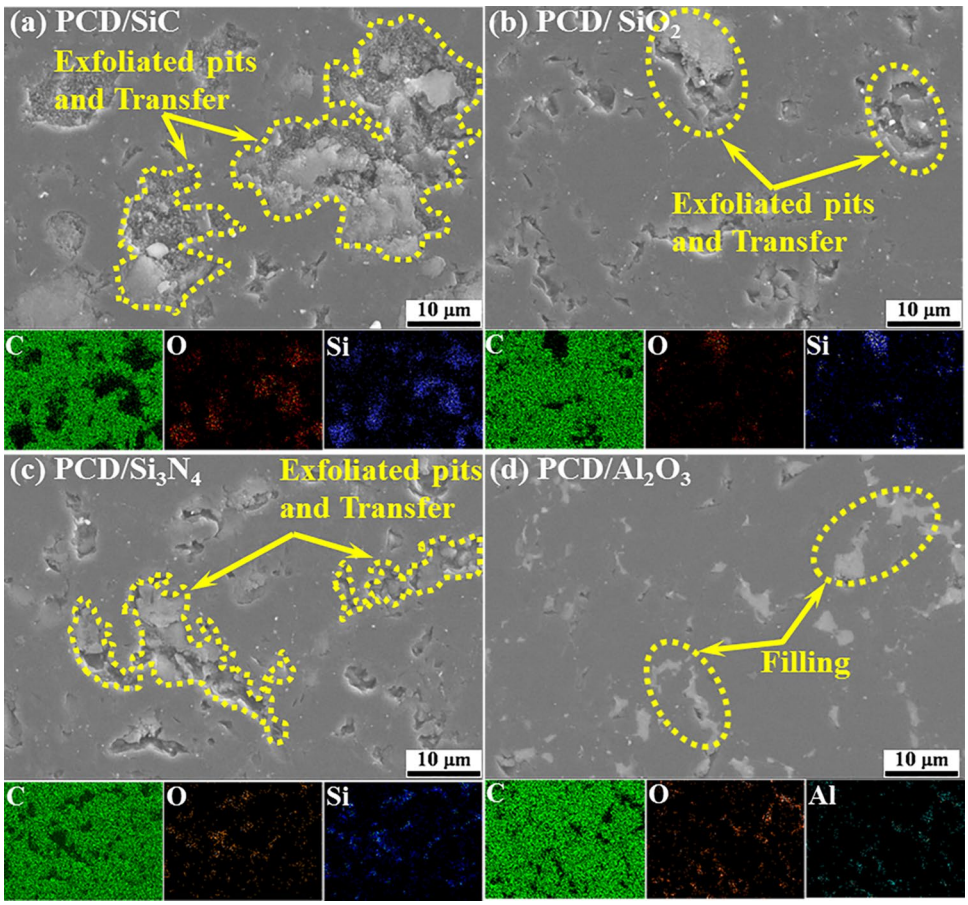

Fig. 8 SEM measurements of wear tracks and the corresponding mapping results. The material transfer phenomena and filling effects were highlighted

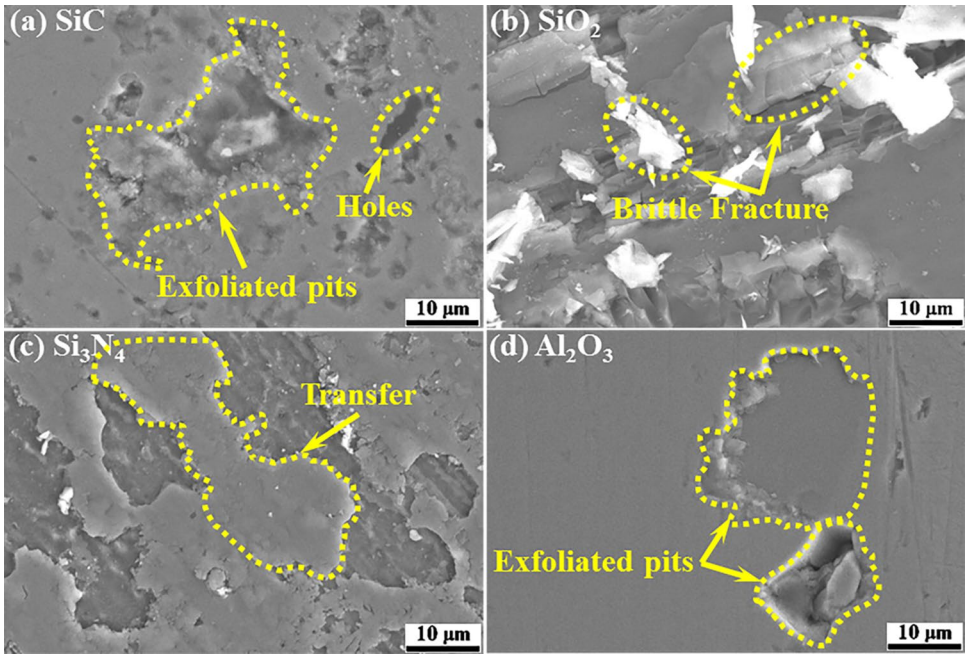

Fig. 9 Typical SEM morphologies of wear scars

(Fig. 8d). EDS mapping results further demonstrate the transfer phenomenon and filling effects.

Figure 9 illustrates the microstructures of wear scars. Figure 9a shows obvious exfoliated pits for SiC ball, which results in the relative severe wear. As described in Fig. 4, a maximum wear scar formed. For SiO_2, Fig. 9b presents brittle fracture, due to its friability and the high hardness of PCD. As the sliding goes on, the fragments gradually accumulated in the slisding interfaces. Besides, the incomplete covered transferfilm was found on the wear scar of Si_3N_4 (Fig. 9c). The worn surface on Al_2O_3 wear scar displays a mild wear morphologies, only a small amount of exfoliated bits can be seen (Fig. 9d). Additionally, the various wear behavior of those mating materials lead to the various wear rates as described above.

4 Discussion

The experimental results described above indicate that the COFs, wear rates and the various frictional interface states are controlled by the tribopairs. In the following, the tribological mechanisms will be discussed in details. Although such four mating balls are different in hardness, there is no direct correlation between tribological performance and triboparis. SiO_2 has the lowest hardness in these four types mating balls. But it achieved a relatively high COF and wear rate. Due to its strong brittleness and the cutting action of PCD, the brittle fracture occurs during sliding (see Fig. 9b). The broken fragments exist on sliding interfaces. As a result, from Fig. 3, it shows an increasing COF compared with other counterbodies. Additionally, silica can play a role of a catalytic function and it increases the reaction rate for C–C bond breaking, which can aid in the wear of diamond [27]. In the case of Al_2O_3 as tribopair, lower friction coefficient and wear rate were achieved. Generally, for dry sliding interfaces, the high friction coefficient is governed by the surface roughness of the sliding interfaces during initial sliding cycles [28, 29]. However, the interfacial filling effect can decrease the roughness and the shear effect was diminished, which can play an effective role in reducing friction and wear. As shown in Fig. 8d, there are obvious filling effects on the micro-cracks and exfoliated pits at the sliding interface, which results in a relatively flat surface. Furthermore, during sliding, it is hardly possible for chemical bonds forming due to the weak affinity between Al and C elements [30–32]. So, the interfacial adhesion effect decreased and then the wear debris can be effectively filled in holes, which results in an enhanced tribological performance.

During initial sliding passes, the flash temperature cannot be avoided among the asperity regions [5], which can influence the initial physical adsorbent species and the rehybridization process [33–36]. It can lead to a loss of initial passivating species such as –H or –OH, and the dangling bonds are subsequently exposed. Additionally, the flash temperature rise (ΔT) between asperities can be estimated by the following formula [4, 37]:

$$\Delta T = \frac{\mu F_n v}{4\alpha\left(K_{\mathrm{PCD}} + K_{\mathrm{Mating\ materials}}\right)}$$

where ΔT is the flash temperature rise, μ is the coefficient of friction, F_n is the applied normal load, v is the sliding

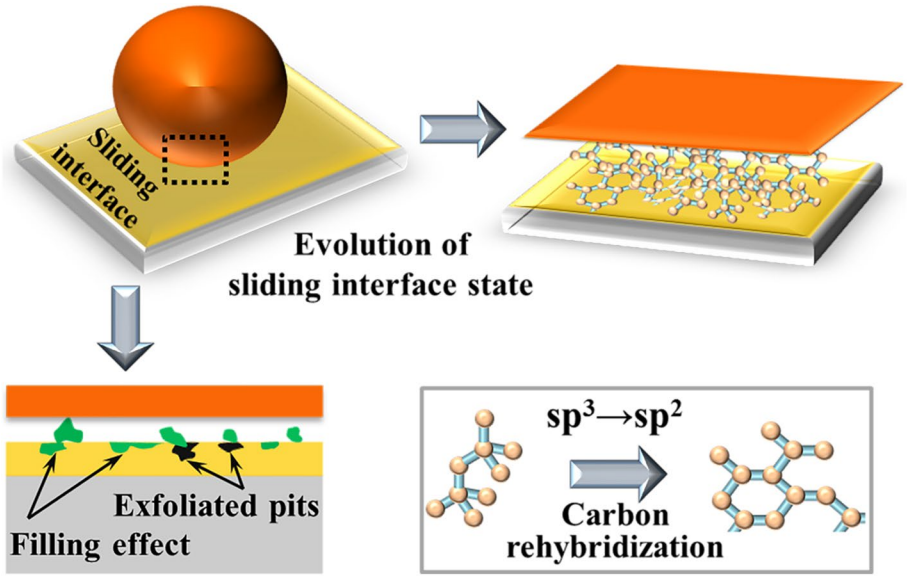

Fig. 10 Schematic diagram of the evolution of sliding interfaces

velocity, α is the contact radius of the real contact area, and K_{PCD} and $K_{Mating\ materials}$ are the thermal conductivities of the PCD and mating materials, respectively. For Si_3N_4, due to the minimum thermal conductivity the relatively high μ value in running-in periods, the contact interfaces may generate the relatively high flash temperature as sliding continues [4, 9, 25, 38]. The relatively high flash temperature can accelerate the carbon rehybridization [4, 5, 9, 39]. Based on this, an easier sp^3-to-sp^2 rehybridization can be observed for PCD/Si_3N_4. Additionally, under dry N_2 atmospheres, the absence of passivating species, the unsaturated carbon can be able to bond to the counterface. Furthermore, mechanically induced desorption creates dangling carbon bonds formation, which can increase friction and wear due to interfacial bonding effect [40]. The strong covalent interaction effects result in a relatively higher wear rates for SiC and Si_3N_4. As described in Fig. 7a, the Raman measurement on wear scar of SiC and Si_3N_4 indicates that there is a process of rehybridization occurred for PCD surface with the carbonaceous transferfilm formation on its wear scars. In the case of SiC as counterbody, the wear rate was the highest among all the mating balls. Since Si atom is easy to covalent with C atom in diamond, high shear strength emerged during the sliding process, causing the disorder of diamond structure. Thus, graphitization [41–43] occurred at sliding interface (see Fig. 7), together with the reduction of friction coefficient. For PCD/Si_3N_4 and PCD/SiC, the I_D/I_G ratios (where I_D and I_G are the Raman intensities of D-peak and G-peak) [44, 45] were calculated with the value of ~ 0.73 and ~ 1.22, respectively. An increased I_D/I_G ratio indicates more disorder in the carbon network. However, both graphitic or amorphous carbon material formed at sliding interfaces have been demonstrated that they can play an effective role in reducing the friction coefficient [19, 21]. Disordered structure results in the decrease of diamond strength, contributing to the exfoliation of the unstable diamond particles (see Fig. 8). Besides, the strong covalence effect is detrimental to wear behavior of PCD. For worn surface of PCD, the interferometry results display the macroscopic wear morphologies, which highlights the exfoliation phenomena and SEM measurements show the exfoliation of diamond particles in details.

Figure 10 describes the schematic diagram of the evolution of frictional interface states. For Si_3N_4 mating ball, it shows a low and stable friction coefficient. During sliding, strong covalent coupling action of Si and C atom results in the break of C–C in diamond and generates a disordered surface with the carbonaceous transferfilm, which is corresponding to carbon rehybridization [46]. As shown in Fig. 10, for Al_2O_3, the filling effect can result in the decrease of roughness, which may induce the enchanced tribological performance [28]. The evolution of frictional interface states is related to the formation of transferfilm and filling effects, which can work a lot in friction-reduction. The results indicate that PCD processes a complicated tribological property when sliding against different mating materials, during which the carbon rehybridization is accompanied at sliding interfaces, which seriously affects the overall tribological performance.

5 Conclusions

A series of experiments were conducted to evaluate the friction and wear behavior of PCD sliding against different mating materials under dry N_2 conditions. The results can be concluded as follows:

(1) The lower steady-state friction coefficients are attributed to the effects of the interfacial filling effects and the formation of transferfilm, which is controlled by the tribopairs.
(2) The carbon rehybridization accompanying with the formation interfacial transferfilm is beneficial to the friction reduction.
(3) Carbon rehybridization deteriorates the bonding strength of diamond bonds and then the main wear loss is caused by the exfoliation of fine diamond grains under the high shear stress conditions during sliding.

Acknowledgements This work was financially supported by the National Natural Science Foundation of China (51875537, 41572359, 51375466), Beijing Natural Science Foundation (3172026, 3182032), Beijing Nova Program (Z171100001117059) and the Fundamental Research Funds for the Central Universities (2652018112).

References

1. Knuteson, C.W., Sexton, T.N., Cooley, C.H.: Wear-in behavior of polycrystalline diamond thrust bearings. Wear **271**, 2106–2110 (2011)
2. Qin, W.B., Yue, W., Wang, C.B.: Understanding integrated effects of humidity and interfacial transfer film formation on tribological behaviors of sintered polycrystalline diamond. RSC Adv. **5**, 53484–53496 (2015)
3. Lingwall, B.A., Sexton, T.N., Cooley, C.H.: Polycrystalline diamond bearing testing for marine hydrokinetic application. Wear **302**, 1514–1519 (2013)
4. Zhao, Y.H., Yue, W., Lin, F., Wang, C.B., Wu, Z.Y.: Friction and wear behaviors of polycrystalline diamond under vacuum conditions. Int. J. Refract. Met. Hard Mater. **50**, 43–52 (2015)
5. Liu, Y., Meletis, E.I.: Evidence of graphitization of diamond-like carbon films during sliding wear. J. Mater. Sci. **32**, 3491–3495 (1997)
6. Huang, Y.H., Yao, Q.Z., Qi, Y.Z., Cheng, Y., Wang, H.T., Li, Q.Y., et al.: Wear evolution of monolayer graphene at the macroscale. Carbon **115**, 600–607 (2017)
7. Li, J.S., Yue, W., Qin, W.B.: Approach to controllable tribological properties of sintered polycrystalline diamond compact through annealing treatment. Carbon **116**, 103–112 (2017)
8. Gardos, M.N., Soriano, B.L.: The effect of environment on the tribological properties of polycrystalline diamond films. J. Mater. Res. **5**, 2599–2609 (1990)
9. Liu, Y.Y., Yue, W., Qin, W.B., Wang, C.B.: Improved vacuum tribological properties of sintered polycrystalline diamond compacts treated by high temperature annealing. Carbon **124**, 651–661 (2017)
10. Ajikumar, P.K., Ganesan, K., Kumar, N., Ravindran, T.R., Kalavathi, S., Kamruddin, M.: Role of microstructure and structural disorder on tribological properties of polycrystalline diamond films. Appl. Surf. Sci. **469**, 10–17 (2019)
11. Sha, X.H., Yue, W., Qin, W.B., Wang, C.B.: Enhanced tribological behaviors of sintered polycrystalline diamond by annealing treatment under humid condition. Int. J. Refract. Met. Hard Mater. **80**, 85–96 (2019)
12. Liu, C., Man, Z.Y., Zhou, F.B., Chen, K., Yu, H.Y.: The wear and friction characters of polycrystalline diamond under wetting conditions. J. Tribol. **141**, 021607 (2019)
13. Qin, W.B., Yue, W., Wang, C.B.: Controllable wear behaviors of silicon nitride sliding against sintered polycrystalline diamond via altering humidity. J. Am. Ceram. Soc. **101**, 2506–2515 (2018)
14. Gosvami, N.N., Bares, J.A., Mangolini, F., Konicek, A.R., Yablon, D.G., Carpick, R.W.: Mechanisms of antiwear tribofilm growth revealed in situ by single-asperity sliding contacts. Science **348**, 102–106 (2015)
15. Berman, D., Deshmukh, S.A., Sankaranarayanan, S.K.R.S., Erdemir, A., Sumant, A.V.: Macroscale superlubricity enabled by graphene nanoscroll formation. Science **348**, 1118–1122 (2015)
16. Erdemir, A., Ramirez, G., Eryilmaz, O.L., Narayanan, B., Liao, Y., Kamath, G., et al.: Carbon-based tribofilms from lubricating oils. Nature **536**, 67 (2016)
17. Berman, D., Erdemir, A., Sumant, A.V.: Reduced wear and friction enabled by graphene layers on sliding steel surfaces in dry nitrogen. Carbon **59**, 167–175 (2013)
18. Berman, D., Erdemir, A., Sumant, A.V.: Few layer graphene to reduce wear and friction on sliding steel surfaces. Carbon **54**, 454–459 (2013)
19. Chen, X.C., Zhang, C.H., Kato, T., Yang, X.A., Wu, S., Wang, R., et al.: Evolution of tribo-induced interfacial nanostructures governing superlubricity in a-C:h and a-C:H:Si films. Nat. Commun. **8**, 1675 (2017)
20. Manimunda, P., Al-Azizi, A., Kim, S.H., Chromik, R.R.: Shear-induced structural changes and origin of ultralow friction of hydrogenated diamond-like carbon (DLC) in dry environment. ACS Appl. Mater. Inter. **9**, 16704–16714 (2017)
21. Rani, R., Panda, K., Kumar, N., Titovich, K.A., Ivanovich, K.V., Vyacheslavovich, S.A.: Tribological properties of ultrananocrystalline diamond films: mechanochemical transformation of sliding interfaces. Sci. Rep. **8**, 283 (2018)
22. Waesche, R., Hartelt, M., Weihnacht, V.: Influence of counterbody material on wear of ta-c coatings under fretting conditions at elevated temperatures. Wear **267**, 2208–2215 (2009)
23. Liu, H.W., Tanaka, A., Kumagai, T.: Influence of sliding mating materials on the tribological behavior of diamond-like carbon films. Thin Solid Films **352**, 145–150 (1999)
24. Wang, Y.G., Liu, B., Song, J.Y., Yan, X.P., Wu, K.M.: Study on the wear mechanism of PCD tools in high-speed milling of Al-Si alloy. Adv. Mater. Res. **381**, 16–19 (2011)
25. Hisakado, T., Tani, H.: Effects of elevated temperatures and topographies of worn surfaces on friction and wear of ceramics in vacuum. Wear **224**, 165–172 (1999)
26. Pastewka, L., Moser, S., Moseler, M.: Atomistic insights into the running-in, lubrication, and failure of hydrogenated diamond-like carbon coatings. Tribol. Lett. **39**, 49–61 (2010)
27. Uetsuka, H., Pastewka, L., Moseler, M.: Activation and mechanochemical breaking of C-C bonds initiate wear of diamond (110) surfaces in contact with silica. Carbon **98**, 474–483 (2016)
28. Radhika, R., Kumar, N., Dash, S., Ravindran, T.R., Arivuolia, D., Tyagi, A.K.: Friction mechanism in diamond-like carbon film sliding against various counterbodies. Mater. Tech. **29**, 366–371 (2014)
29. Mo, Y., Turner, K.T., Szlufarska, I.: Friction laws at the nanoscale. Nature **457**, 1116 (2009)
30. Warrier, S.G., Blue, C.A., Lin, R.Y.: Control of interfaces in Al–C fibre composites. J. Mater. Sci. **28**, 760–768 (1993)
31. Soukup, R.W.: Historical aspects of the chemical bond chemical relationality versus physical objectivity. Monatshefte für Chemie/Chemical Monthly **136**, 803–818 (2005)
32. Pan, Y., Liu, X., Yang, H.: Role of C and Fe in grain refinement of an AZ 63 B magnesium alloy by Al–C master alloy. J. Mater. Sci. Technol. **21**, 822–826 (2005)
33. Salivati, N., Ekerdt, J.G.: Temperature programmed desorption studies of deuterium passivated silicon nanocrystals. Surf. Sci. **603**, 1121–1125 (2009)

34. Konicek, A.R., Grierson, D.S., Sumant, A.V., Friedmann, T.A., Sullivan, J.P., Gilbert, P.U.P.A., et al.: Influence of surface passivation on the friction and wear behavior of ultrananocrystalline diamond and tetrahedral amorphous carbon thin films. Phys. Rev. B **85**, 543–548 (2012)
35. Panczyk, T., Rudzinski, W.: A statistical rate theory approach to kinetics of dissociative gas adsorption on solids. J. Phys. Chem. B **108**, 2898–2909 (2004)
36. Alcañiz-Monge, J., Linares-Solano, A., Rand, B.: Water adsorption on activated carbons: study of water adsorption in micro-and mesopores. J. Phys. Chem. B **105**, 7998–8006 (2001)
37. Rabinowicz, E.: Friction and wear of materials, 2nd edn. Wiley, New York, NY (1995)
38. Zeiler, E., Klaffke, D., Hiltner, K., Grögler, T., Rosiwal, S.M., Singer, R.F.: Tribological performance of mechanically lapped chemical vapor deposited diamond coatings. Surf. Coat. Technol. **116**, 599–608 (1999)
39. Ma, T.B., Hu, Y.Z., Wang, H.: Molecular dynamics simulation of shear-induced graphitization of amorphous carbon films. Carbon **47**, 1953–1957 (2009)
40. Gao, G.T., Mikulski, P.T., Chateauneuf, G.M., Harrison, J.A.: The effects of film structure and surface hydrogen on the properties of amorphous carbon films. J. Phys. Chem. B **107**, 11082–11090 (2003)
41. Eryilmaz, O.L.: Tof-SIMS and XPS characterization of diamond-like carbon films after tests in inert and oxidizing environments. Wear **265**, 244–254 (2008)
42. Chen, J., Deng, S.Z., Chen, J., Yu, Z.X., Xu, N.S.: Graphitization of nanodiamond powder annealed in argon ambient. Appl. Phys. Lett. **74**, 3651–3653 (1999)
43. Wang, C.Z., Ho, K.M., Shirk, M.D., Molian, P.A.: Laser-induced graphitization on a diamond (111) surface. Phys. Rev. Lett. **85**, 4092 (2000)
44. Hovsepian, P.E., Mandal, P., Ehiasarian, A.P., Sáfrán, G., Tietema, R., Doerwald, D.: Friction and wear behaviour of Mo–W doped carbon-based coating during boundary lubricated sliding. Appl. Surf. Sci. **366**, 260–274 (2016)
45. Pachfule, P., Shinde, D., Majumder, M., Xu, Q.: Fabrication of carbon nanorods and graphene nanoribbons from a metal–organic framework. Nat. Chem. **8**, 718 (2016)
46. Grierson, D.S., Sumant, A.V., Konicek, A.R., Friedmann, T.A., Sullivan, J.P., Carpick, R.W.: Thermal stability and rehybridization of carbon bonding in tetrahedral amorphous carbon. J. Appl. Phys. **107**, 033523 (2010)